nature methods

ARTICLES

https://doi.org/10.1038/s41592-019-0329-7

One-step generation of modular CAR-T cells with AAV–Cpf1

Xiaoyun Dai[1,2,3,8], Jonathan J. Park[1,2,3,4,8], Yaying Du[1,2,3], Hyunu R. Kim[1,2,3], Guangchuan Wang[1,2,3], Youssef Errami[1,2,3] and Sidi Chen[1,2,3,4,5,6,7*]

Immune-cell engineering opens new capabilities for fundamental immunology research and immunotherapy. We developed a system for efficient generation of chimeric antigen receptor (CAR)-engineered T cells (CAR-T cells) with considerably enhanced features by streamlined genome engineering. By leveraging trans-activating CRISPR (clustered regularly interspaced short palindromic repeats) RNA (tracrRNA)-independent CRISPR–Cpf1 systems with adeno-associated virus (AAV), we were able to build a stable CAR-T cell with homology-directed-repair knock-in and immune-checkpoint knockout (KIKO CAR-T cell) at high efficiency in one step. The modularity of the AAV–Cpf1 KIKO system enables flexible and highly efficient generation of double knock-in of two different CARs in the same T cell. Compared with Cas9-based methods, the AAV–Cpf1 system generates double-knock-in CAR-T cells more efficiently. CD22-specific AAV–Cpf1 KIKO CAR-T cells have potency comparable to that of Cas9 CAR-T cells in cytokine production and cancer cell killing, while expressing lower levels of exhaustion markers. This versatile system opens new capabilities of T-cell engineering with simplicity and precision.

Genome engineering in human primary T cells holds promise for the development of novel immunotherapeutics[1–5]. Genetically modified T cells expressing CARs have recently been approved for the treatment of B-cell lymphoma and leukemia[6–8]. Currently approved CAR-T cell transgene delivery is based on randomly integrating lentiviral and γ-retroviral vectors, which carries the risk of insertional oncogenesis and translational silencing[9,10]. Targeted integration of CD19 CAR into the T cell receptor-α constant (*TRAC*) gene locus by CRISPR–Cas9 showed higher efficacy in a mouse model of acute lymphoblastic leukemia (ALL) compared with conventionally generated CAR-T cells[11]. Recent methods to modify human T cells are based on Cas9 ribonucleoproteins (RNPs)[12], which can be combined with viral or non-viral templates[13,14]. CRISPR–Cas9 systems also enable editing of endogenous loci to minimize graft-versus-host reactions mediated by T-cell receptor (TCR) or human leukocyte antigen[15,16]. Clinical studies are ongoing to test the effects of programmed cell death 1 (*PDCD1/PD-1*) gene knockout in CAR-T cells for multiple myeloma or solid tumors (for example, NCT03399448 and NCT03545815). Although multiplex gene editing in CAR-T cells is possible with Cas9, it requires lentiviral transduction followed by electroporation of multiple components including Cas9 protein, guide RNAs produced in vitro, and homology-directed repair (HDR) template[15,16], which complicates the manufacturing process. Better approaches to streamline multilocus genome editing and achieve improved effector CAR-T cell function are of vital importance for human cell therapies.

Cas12a/Cpf1, a class 2 type V CRISPR system, is a multi-potent effector that can process CRISPR RNA (crRNA) arrays by itself and mediate DNA cleavage at multiple targets using a single customized CRISPR array[17–19]. In contrast to Cas9, Cpf1 is tracrRNA independent and requires only a crRNA that consists of a 20–23-nucleotide protospacer and a direct repeat[17–19]. Compared with Cas9, Cpf1 has higher specificity in human cells, potentially owing to its biochemical characteristics, and generates sticky-end double-stranded breaks that are less prone to non-homologous end joining (NHEJ), which makes them ideal for precise gene editing[17–19]. Given these advantages, we set out to develop a platform for precise targeting of multiple loci in human primary T cells based on Cpf1. Using a combination of messenger RNA electroporation for LbCpf1 (Cpf1 from *Lachnospiraceae*) and AAV6 for delivery of crRNA and HDR template (the combined system is hereinafter referred to as AAV–Cpf1), we achieved simple yet highly efficient targeting of both HDR-mediated dual-CAR knock-in and immune-checkpoint gene knockout (KIKO for short) in primary human T cells. KIKO CAR-T cells generated by the AAV–Cpf1 platform have multiple advantageous features such as CAR retention, cancer cell killing, effector function, and resistance to exhaustion. This enables highly efficient generation of advanced CAR-T cells to streamline the creation of more complex genetically engineered T cells by modular processing.

Results

High-efficiency multiplexed genome editing with AAV–Cpf1 in human primary T cells. We optimized a workflow using AAV–Cpf1 for human primary T-cell engineering (Fig. 1a). We delivered a pseudouridine-modified LbCpf1 mRNA with 5′ cap and poly(A) tail into human CD4$^+$ T cells[20], and confirmed the expression of LbCpf1 protein that peaked on day 1 postelectroporation and diminished on day 4 (Supplementary Fig. 1a). Using an AAV vector carrying a U6-promoter-driven Cpf1 crRNA targeting the 5′ end of the first exon of *TRAC* (crTRAC) (Supplementary Fig. 1b), we titrated the targeting efficiency of AAV–Cpf1 with two AAV serotypes (AAV9 and AAV6) for packaging. Fluorescence-activated cell sorting (FACS) analysis showed that both AAV9 and AAV6 carrying crTRAC reduced TCR$^+$ T cells in a multiplicity of infection

[1]System Biology Institute, Yale University, West Haven, CT, USA. [2]Department of Genetics, Yale University School of Medicine, New Haven, CT, USA. [3]Center for Cancer Systems Biology, Integrated Science & Technology Center, Yale University, West Haven, CT, USA. [4]Yale MD–PhD Program, Yale University, New Haven, CT, USA. [5]Immunobiology Program, Yale University, New Haven, CT, USA. [6]Yale Comprehensive Cancer Center, Yale University, New Haven, CT, USA. [7]Yale Stem Cell Center, Yale University, New Haven, CT, USA. [8]These authors contributed equally: Xiaoyun Dai, Jonathan J. Park. *e-mail: sidi.chen@yale.edu

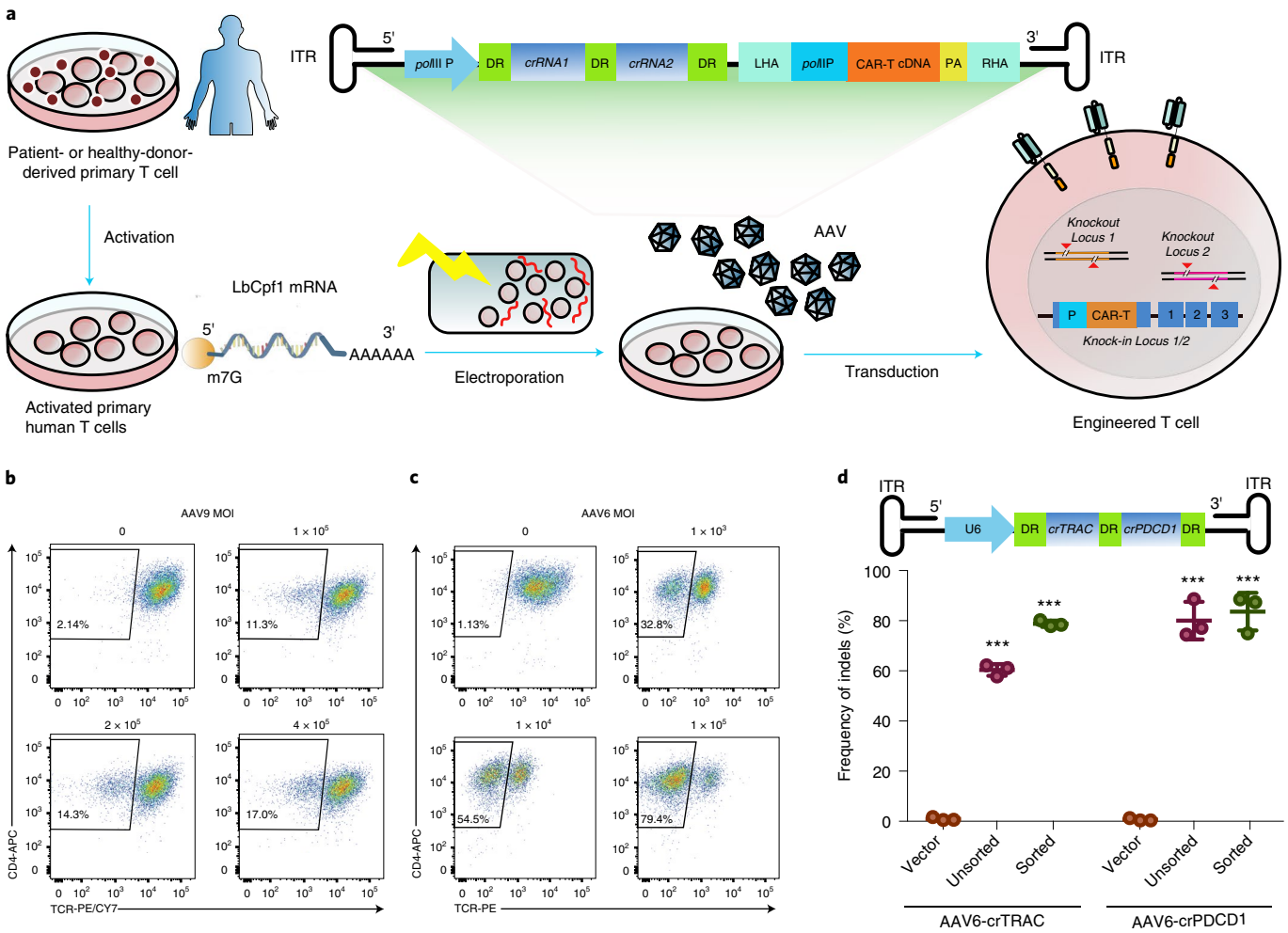

Fig. 1 | AAV-Cpf1-mediated efficient multiplexed genome editing in human primary CD4⁺ T cells. a, Schematic of LbCpf1 mRNA electroporation combined with AAV-delivered crRNA and HDR template (AAV-Cpf1), enabling knockout and knock-in of different genes in human primary T cells. **b**,**c**, Efficiency of AAV9-mediated (**b**) and AAV6-mediated (**c**) TCR knockout on human primary CD4⁺ T cells using FACS. One representative sample's data are shown for 1–5 biological replicates as indicated in Supplementary Fig. 1c. **d**, Top, schematic of a double-knockout AAV6-crRNA array targeting *PDCD1* and *TRAC*. Bottom, quantification of the frequency of CRISPR-Cpf1-mediated double knockout of *PDCD1* and *TRAC* from human primary CD4⁺ T cells after AAV6 infection for 5 d ($n = 3$ independent infection replicates). Unpaired two-sided *t*-test was used to assess significance. Knockout versus vector, $^{***}P < 0.001$ for all comparisons. Precise *P* values, up to the precision of 1×10^{-15}, are provided in Supplementary Data 1, similarly thereafter. Data are shown as mean ± s.e.m., plus individual data points on the graph. ITR, inverted terminal repeat.

(MOI)-dependent manner, with higher efficiency by AAV6 (Fig. 1b,c and Supplementary Fig. 1c). With Illumina Nextera amplicon library prep, next-generation sequencing (NGS) analysis showed on-target mutagenesis at the DNA level as evident by insertions and deletions (indels), which is also MOI dependent (Supplementary Fig. 1d). We constructed an AAV vector carrying a crRNA array targeting both *TRAC* and *PDCD1* loci (crTRAC;crPDCD1), and showed that one transduction simultaneously generated editing in both loci using either AAV9 or AAV6, with the latter having high efficiency (Supplementary Fig. 2a–d). With AAV6–crTRAC;crPDCD1, NGS quantification showed that mutation efficiencies at *TRAC* and *PDCD1* loci in bulk unsorted cells reached 60.39% and 80.07%, respectively (Fig. 1d), which was further enriched by FACS on the TCR⁻ population (78.80% and 83.63%, respectively) (Fig. 1d). These data demonstrated that AAV6 delivery of crRNA array with LbCpf1 mRNA electroporation is an efficient means for multiplexed editing in human primary T cells.

Modular and simultaneous knock-in and knockout in human primary T cells. We then leveraged the AAV vector to simultaneously deliver HDR template and crRNA array. We first tested knock-in of the reporter gene *dTomato* into *TRAC* with simultaneous *PDCD1* knockout, using a single AAV construct, *PDCD1*^{KO};*dTomato-TRAC*^{KI} (*TRAC*-KIKO) (Fig. 2a and Supplementary Fig. 3a). Five days after electroporation and transduction, *TRAC*-KIKO mediated efficient, targeted *dTomato* integration as measured by flow cytometry (Fig. 2a). By staining CD3 that forms a surface complex with TCR[21], we detected TRAC:CD3 knockdown efficiency at >70%, with on-target integration of *dTomato* at >40% of total CD4⁺ T cells (Fig. 2a and Supplementary Fig. 4a). We used a semiquantitative In-Out PCR and confirmed *dTomato-TRAC* integration at the DNA level, with bulk HDR efficiency at 34.7% in unsorted cells and enriched to 69.5% in CD3⁻dTomato⁺ -sorted cells by gel quantification (Supplementary Fig. 3b). NGS revealed the HDR junctions (Supplementary Fig. 3c), and also quantified the *dTomato-TRAC* HDR at 42.18% and 72.84% in bulk and enriched populations, respectively, with simultaneous measurements of *TRAC* wild-type (WT) and NHEJ alleles (Supplementary Fig. 3d). In the same samples, *PDCD1* knockout as indels at the predicted cleavage sites were also observed at bulk frequencies of 47% and 72% by

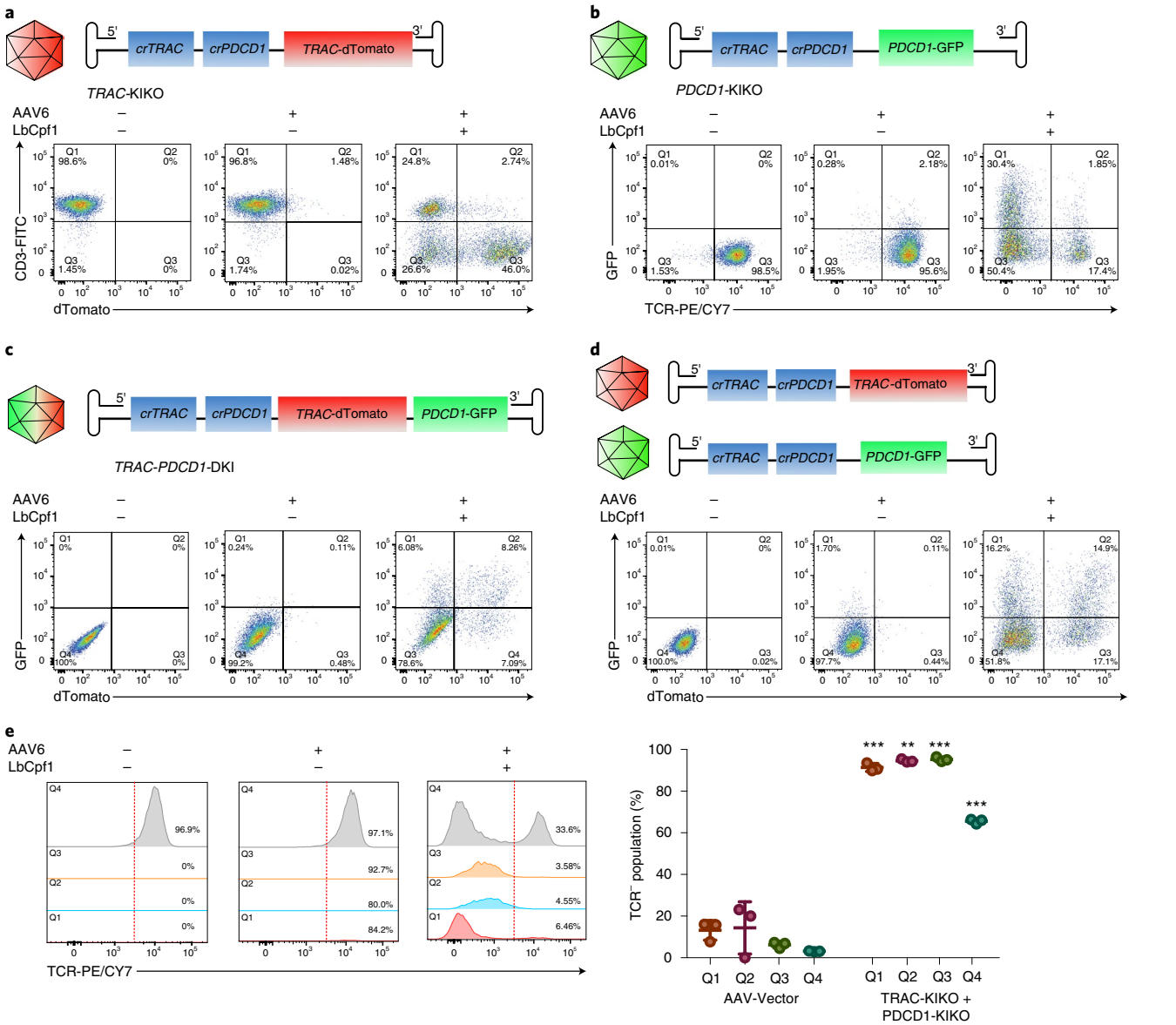

Fig. 2 | Modular combinations of AAV–Cpf1-mediated efficient multiplex knock-in and knockout in human primary CD4⁺ T cells. a, AAV–Cpf1-mediated *dTomato* transgene knock-in into the *TRAC* locus with *PDCD1* knockout. Top, schematics of construct design for *PDCD1*^{KO};*dTomato-TRAC*^{KI} (*TRAC*-KIKO). Bottom, flow cytometry plots showing representative *TRAC* dTomato knock-in 5 d after AAV transduction (AAV6 packaging, MOI = 1×10^5). Experiments were done with three infection replicates; quantifications and statistics are shown in Supplementary Fig. 4a. **b**, AAV–Cpf1-mediated GFP transgene knock-in into *PDCD1* locus with *TRAC* knockout. Top, schematics of construct design for *TRAC*^{KO};*GFP-PDCD1*^{KI} (*PDCD1*-KIKO). Bottom, flow cytometry plots showing representative *PDCD1* GFP knock-in 5 d after AAV transduction (AAV6 packaging, MOI = 1×10^5). Experiments were done with six infection replicates; quantifications and statistics are shown in Supplementary Fig. 4b. **c**, AAV–Cpf1-mediated double knock-in with a single vector. Top, schematics of construct design for double-knock-in AAV vector *dTomato-TRAC*^{KI};*GFP-PDCD1*^{KI} (TRAC-PDCD1-DKI), where dTomato and GFP are targeted to be integrated into the *TRAC* locus and the *PDCD1* locus, respectively. Bottom, representative flow cytometry plots showing double knock-in 5 d after transduction of a single AAV construct (AAV6 packaging, MOI = 1×10^5). Experiments were done with 3–4 infection replicates; quantifications and statistics are shown in Supplementary Fig. 4c. **d**, AAV–Cpf1-mediated double knock-in with a two-vector system. Top, schematics of construct design for using both *PDCD1*^{KO};*dTomato-TRAC*^{KI} and *TRAC*^{KO};*GFP-PDCD1*^{KI} for dual targeting. Bottom, representative flow cytometry plots showing double knock-in 5 d after transduction of both AAV constructs (AAV6 packaging, MOI = 1×10^5). Experiments were done with three infection replicates; quantifications and statistics are shown in Supplementary Fig. 4d. **e**, Analysis of TCR-knockout efficiency in knock-in cells by FACS. Left, representative flow cytometry plots of the TCR expression levels in non-integration (Q4), single-integration (Q1, Q3), or double-integration (Q2) T cells from the two-vector system. An example workflow of FACS gating plots is shown in Supplementary Fig. 13. Right, quantification of TCR⁻ percentages in different quadrants shown in column graph (infection replicates, $n = 3$). Unpaired two-sided *t*-test was used to assess significance. TCR⁻ population, vector versus dual targeting, $^{**}P < 0.01$, $^{***}P < 0.001$. Data are shown as mean ± s.e.m.

T7E1 (NGS 62.34% and 87.03%) in unsorted and TCR⁻dTomato⁺-sorted cells (Supplementary Fig. 3e,f). The T7E1 result is probably an underestimate due to potential homoduplex mutants, especially at high frequency[22]. To test knock-in at sites other than *TRAC*, we generated another KIKO vector, *TRAC*^{KO};*GFP⁻PDCD1*^{KI} (*PDCD1*-KIKO), to knock a green fluorescent protein (GFP) reporter into the

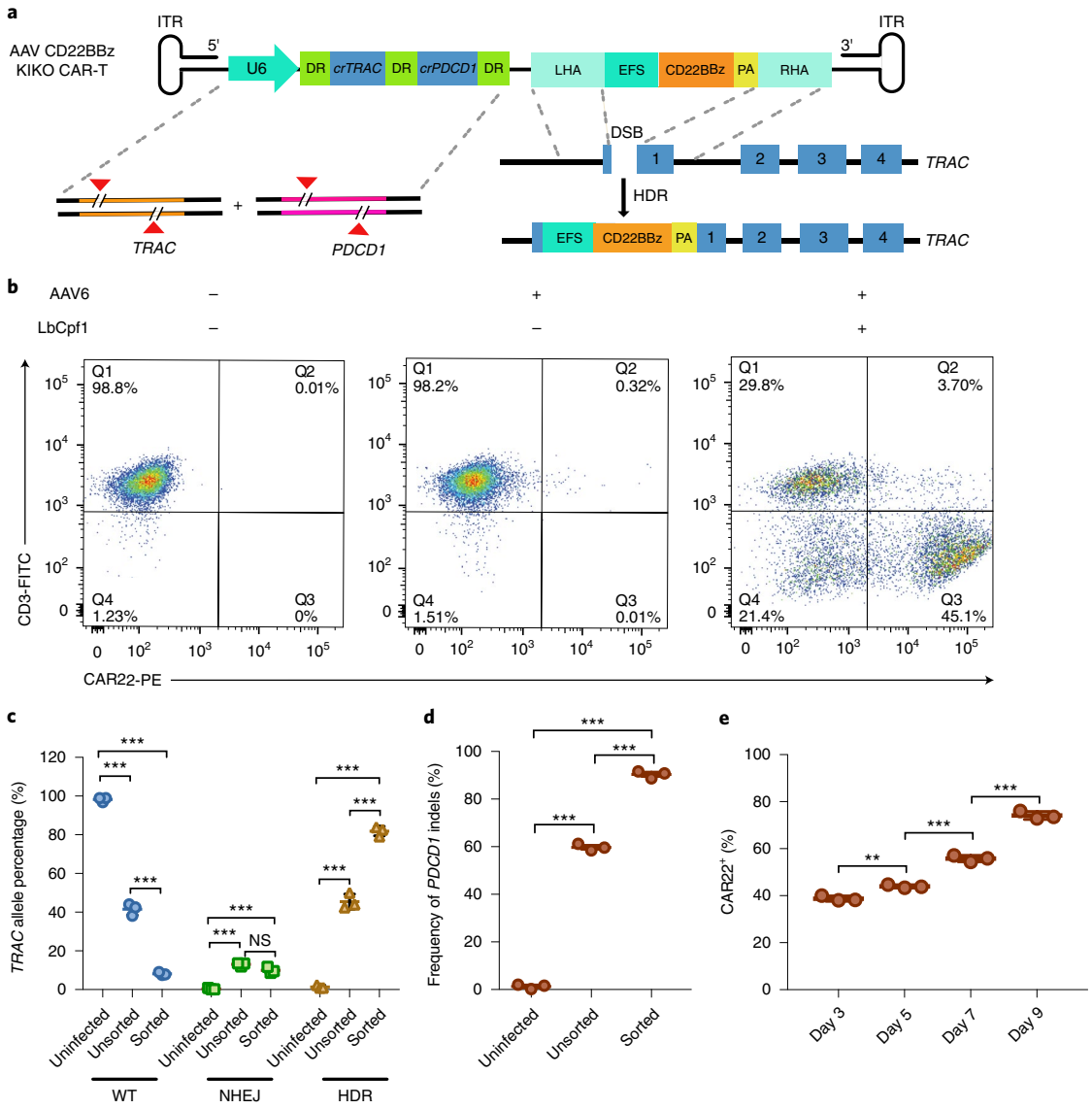

Fig. 3 | High-efficiency generation of stably integrated anti-CD22 CAR-T cells with *PDCD1* knockout by AAV–Cpf1 KIKO in one step. a, Schematic of a single *PDCD1*^{KO};*CD22BBz-TRAC*^{KI} (CD22BBz KIKO) AAV construct for delivering a double-targeting crRNA array and an HDR template mediating *CD22BBz* CAR integration into the *TRAC* locus with *PDCD1* knockout. The HDR template contains an EFS-*CD22BBz* CAR-PA cassette, where the *CD22BBz* CAR transgene is driven by an EFS promoter and terminated by a short poly(A), flanked by two arms homologous to the *TRAC* locus. The AAV vector sample was infected only with AAV6 carrying the same construct, and did not receive electroporation of Cpf1 mRNA thereafter. **b**, Representative flow cytometry plots of human primary CD4$^+$ T cells 5 d after AAV6 transduction (MOI = 1×10^5), showing the detection of *CD22BBz* transgene expression on the T-cell surface only with the AAV–Cpf1 targeting of *PDCD1*^{KO};*CD22BBz-TRAC*^{KI}. Experiments were done with three infection replicates; quantifications and statistics are shown in Supplementary Fig. 6a. **c**, Quantitative allele mapping of *TRAC* locus for *CD22BBz* HDR, NHEJ, and WT reads with $n = 3$ infection replicates. Unpaired two-sided *t*-test was used to assess significance. WT group: vector versus unsorted, $^{***}P < 0.001$; vector versus sorted, $^{***}P < 0.001$; unsorted versus sorted, $^{***}P < 0.001$. NHEJ group: vector versus unsorted, $^{***}P < 0.001$; vector versus sorted, $^{***}P < 0.001$; unsorted versus sorted, not significant (NS). HDR group: vector versus unsorted, $^{***}P < 0.001$; vector versus sorted, $^{***}P < 0.001$; unsorted versus sorted, $^{***}P < 0.001$. Data are shown as mean ± s.e.m. **d**, Quantitative analysis for genomic knockout of *PDCD1* by *PDCD1*^{KO};*CD22BBz-TRAC*^{KI} in human primary CD4$^+$ T cells. Unpaired two-sided *t*-test was used to assess significance. Vector versus unsorted, $^{***}P < 0.001$; vector versus sorted, $^{***}P < 0.001$; unsorted versus sorted, $^{***}P < 0.001$. Data are shown as mean ± s.e.m., plus individual data points on the graph. **e**, Time-course analysis of CAR transgene retention after transduction. CAR22 expression levels of *PDCD1*^{KO};*CD22BBz-TRAC*^{KI} bulk targeted CAR-T cells are shown by dot plot (infection replicates, $n = 3$). The bulk T cells were stimulated once with mitomycin-C-treated NALM6 cells (CD22$^+$; Supplementary Fig. 10a) 5 d after transduction. We measured CAR expression by staining with a specific antibody and then carrying out flow cytometry. One-way ANOVA with Tukey's multiple-comparisons test was used to assess significance. $^{**}P < 0.01$, $^{***}P < 0.001$. Data are shown as mean ± s.e.m., plus individual data points on the graph.

PDCD1 locus while knocking out *TRAC* (Fig. 2b). Similarly, AAV–Cpf1 *PDCD1*-KIKO achieved >80% TCR knockdown with stable GFP integration in near 30% of treated CD4$^+$ T cells (Fig. 2b and Supplementary Fig. 4b).

The capacity to generate double knock-in in the same T cells is essential for multi-feature CAR-T cells such as bispecifics or multiple functional modulators. We then generated a dual-knock-in AAV vector, *dTomato*$^-$*TRAC*^{KI};*GFP-PDCD1*^{KI} (TRAC-PDCD1-DKI),

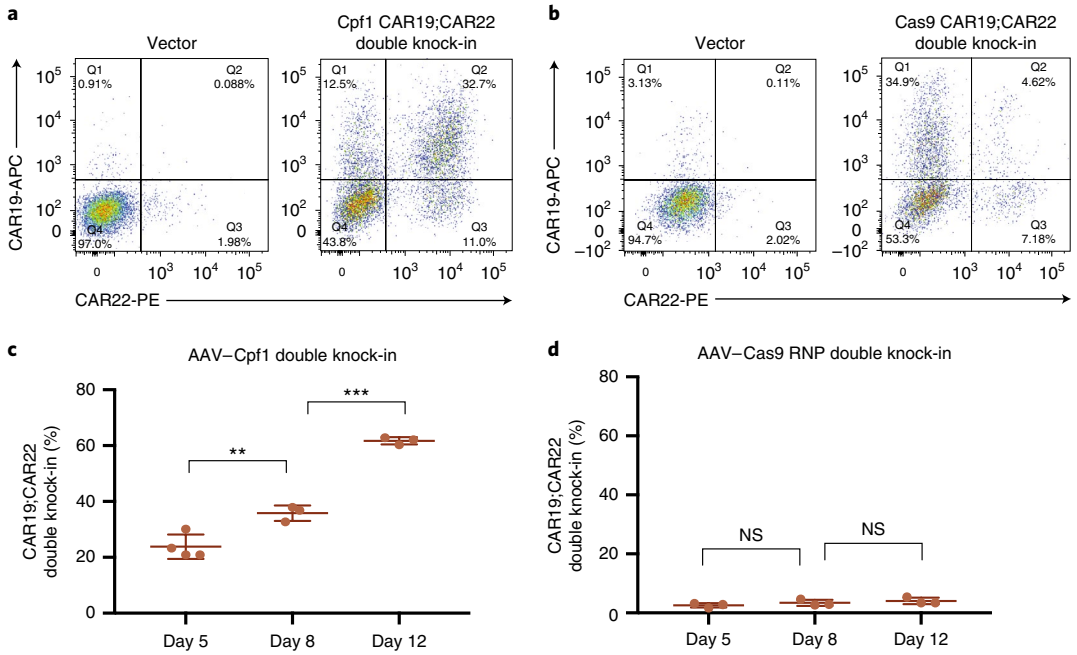

Fig. 4 | AAV–Cpf1 CAR knock-in compared with that achieved by AAV–Cas9. a, Representative flow cytometry plots for AAV–Cpf1-mediated double knock-in with a two-vector system (*PDCD1*^{KO};*CD22BBz-TRAC*^{KI} + *TRAC*^{KO};*CD19BBz-PDCD1*^{KI}) 8 d after transduction of both AAV constructs (AAV6 packaging, MOI = 1×10^5). Experiments were done with three infection replicates; quantifications and statistics are shown in Supplementary Fig. 9a. **b**, Representative flow cytometry plots for AAV–Cas9 RNP-mediated double-knock-in with a two-vector system (two AAVs with CAR19 and CAR22 HDR templates targeting *PDCD1* and *TRAC* loci, respectively) 8 d after transduction of both AAV constructs (AAV6 packaging, MOI = 1×10^5). Experiments were done with 4–6 infection replicates; quantifications and statistics are shown in Supplementary Fig. 9b. **c**, Time-course analysis of double CAR transgene retention after transduction. CAR19 and CAR22 expression levels are shown by dot plot (infection replicates, day 5, $n=4$; day 8 and day 12, $n=3$). One-way ANOVA with Tukey's multiple-comparisons test was used to assess significance. $^{**}P<0.01$, $^{***}P<0.001$. **d**, Time-course analysis of double CAR transgene retention after transduction. CAR19;CAR22 expression levels are shown by dot plot (infection replicates, $n=3$). For both **c** and **d**, bulk T cells were stimulated once with target cells at 5 d post-transduction. Data are shown as mean ± s.e.m., plus individual data points on the graph.

in which dTomato and GFP were targeted for integration into *TRAC* and *PDCD1* loci, respectively. Five days after electroporation and AAV6–TRAC-PDCD1-DKI transduction, 7.54% double-positive GFP$^+$dTomato$^+$ T cells were observed, along with 5.97% GFP and 6.82% dTomato single-positives (Fig. 2c and Supplementary Fig. 4c). An alternative strategy with two different AAV vectors (*PDCD1*^{KO};*dTomato-TRAC*^{KI} and *TRAC*^{KO};*GFP-PDCD1*^{KI}) for dual targeting produced on average 13.83% GFP$^+$dTomato$^+$, 17.23% GFP$^+$, and 16.17% dTomato$^+$ T cells (Fig. 2d and Supplementary Fig. 4d). All of the T cells that underwent integration (including single- and double-positives; Q1, Q2, and Q3) almost completely lost TCR expression, and 65% of non-integration T cells (GFP$^-$dTomato$^-$; Q4) lost TCR expression, whereas vector-transduced T cells mostly retained intact TCR (Fig. 2e). These data demonstrated simple, efficient, and precise double knock-in of transgenes in human T cells by AAV–Cpf1 with crRNA arrays and HDR donors.

One-step generation of *TRAC* knock-in CD22-specific CAR-T cells with *PDCD1* disruption. Integration of anti-CD19 CAR (CAR19) into *TRAC* can improve preclinical efficacy in leukemia, and specific knockouts can reduce T-cell exhaustion[11,23,24]. CD22-CAR targeting B-cell precursor ALL was safe and provided high response rates for pediatric patients who failed chemotherapy and/or CAR19 treatment[25,26]. We generated a single AAV construct, *PDCD1*^{KO};*CD22BBz-TRAC*^{KI} (CD22BBz KIKO, or CAR22 for short) for knocking CAR22 into *TRAC* with *PDCD1* knockout (Fig. 3a). Similarly, we showed that AAV–Cpf1 with CD22BBz KIKO generated precisely targeted knock-in and knockout with limited toxicity and high viability (Fig. 3b and Supplementary Fig. 5a,b). With stimulation, the electroporated T cells quickly expanded over the course of the 26 d observed (Supplementary Fig. 5c). Specifically, 44.6% of these T cells expressed CD22BBz CAR (Fig. 3b and Supplementary Fig. 6a). Semiquantitative In-Out PCR and NGS confirmed CD22BBz integration at the *TRAC* locus, where bulk HDR efficiency with single transduction reached 45.46% in unsorted cells and enriched to 81.88% in CD3$^-$CAR22$^+$-sorted cells (Fig. 3c and Supplementary Fig. 6b,c). NHEJ variants of *TRAC* also existed at 13.01% in bulk and 9.97% in sorted populations on average (Fig. 3c). Simultaneous *PDCD1* knockout was observed at high efficiency at 59.73% in bulk and 90.39% in CD3$^-$CAR22$^+$-sorted T cells on average (Fig. 3d and Supplementary Fig. 6d). Virtually no detectable on-target mutation was found in uninfected control, indicating a clean background. The fraction of CAR22$^+$ T cells steadily increased over time, starting at 38.73% on day 3 and ramping up to 74.13% on day 9 after stimulation with target cells (Fig. 3e and Supplementary Fig. 6e), probably owing to negative selection of non-functional cells. These data demonstrate a simple and rapid method to generate targeted knock-in CAR with simultaneous immune-checkpoint knockout at high efficiency using the AAV–Cpf1 KIKO system in one step.

Modular generation of CD19 and CD22 bispecific CAR-T cells with double knock-in and dual-disruption. We then tested whether AAV–Cpf1 KIKO can efficiently generate more complex CAR-T cells with simple engineering steps. We first generated an AAV vector, *TRAC*^{KO};*CD19BBz-PDCD1*^{KI} (CD19BBz-KIKO), to mediate CD19BBz transgene knock-in into the *PDCD1* locus with *TRAC* knockout (Supplementary Fig. 7a). We found that one transduction could generate CD19BBz-*PDCD1* knock-in at a bulk efficiency of 37.83%, with efficient *TRAC* knockout (Supplementary

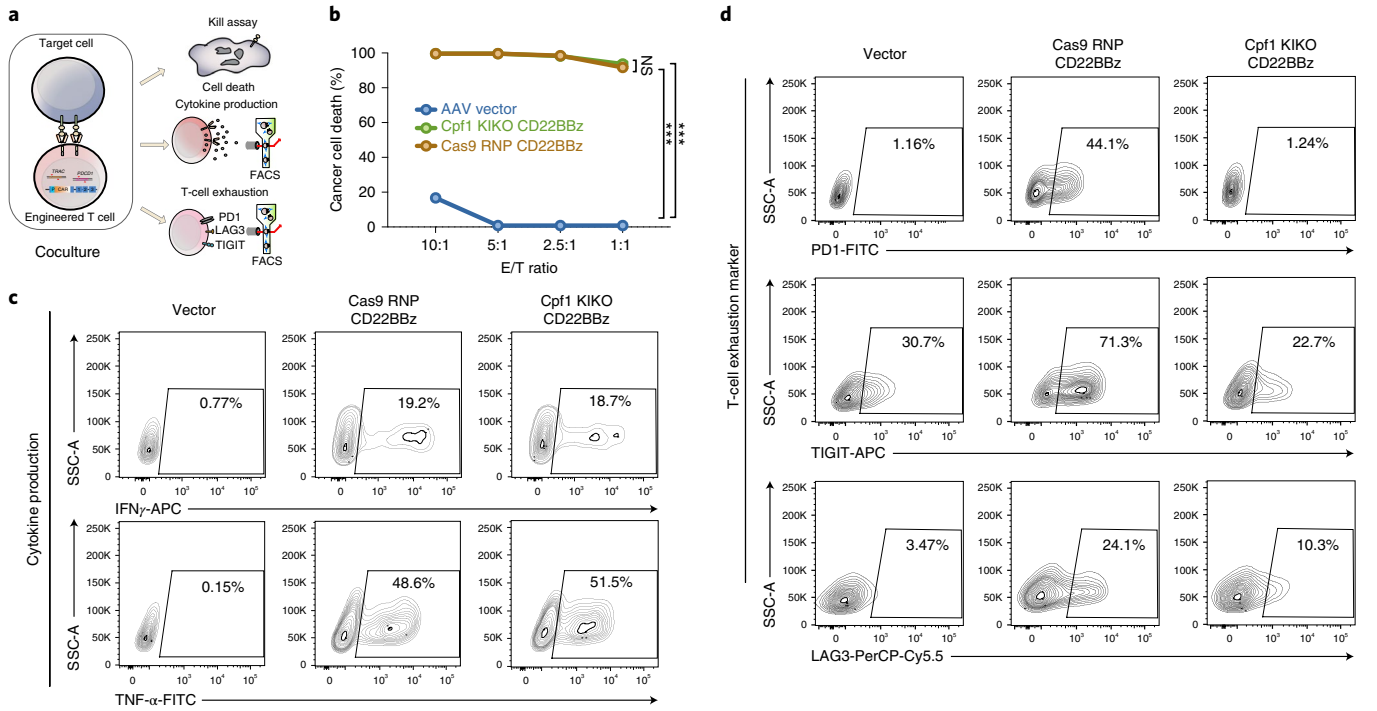

Fig. 5 | Cpf1 CD22BBz KIKO CAR-T cells compared with Cas9-mediated CD22BBz-knock-in and *PDCD1*-knockout CAR-T cells. a, Pipeline for functional testing of Cpf1 CD22BBz KIKO CAR-T cells and Cas9 RNP CD22BBz CAR-T cells. **b**, Comparison of Cpf1 CD22BBz KIKO versus Cas9 RNP CD22BBz CAR-T cells by kill assay. In vitro cytotoxic activity of CAR-T cells on cancer cells was measured by bioluminescence assay at different E/T ratios, using NALM6-GL cells stably transduced with GFP and luciferase genes as target cells (Supplementary Fig. 10b,c). The percentage of cancer cell death is shown for a titration series of E/T ratios for AAV-vector-transduced T cells. Two-way ANOVA with Tukey's multiple-comparisons test was used to assess significance (multiple-testing corrected). Cpf1 CD22BBz CAR versus vector, $^{***}P < 0.001$; Cas9 RNP CD22BBz CAR versus vector, $^{***}P < 0.001$; Cpf1 versus Cas9, NS. **c**, Representative flow cytometry results showing IFN-γ and TNF-α expression levels in Cpf1 CD22BBz KIKO versus Cas9 RNP CD22BBz CAR-T cells. IFN-γ and TNF-α production was tested by intracellular staining after coculture with NALM6 for 5 h at E/T = 1:1. Experiments were done with three infection replicates; quantifications and statistics are shown in Supplementary Fig. 12a. **d**, Representative flow cytometry results showing T-cell exhaustion marker expression level in Cpf1 CD22BBz KIKO versus Cas9 RNP CD22BBz CAR-T cells. PD-1, TIGIT, and LAG3 expression was tested by surface staining after coculture with NALM6 for 24 h at E/T = 0.5:1. Experiments were done with three infection replicates; quantifications and statistics are shown in Supplementary Fig. 12b. All data are shown as mean ± s.e.m., plus individual data points on the graph.

Fig. 7b,c). We then jointly transduced primary CD4$^+$ T cells with both CD22BBz-KIKO and CD19BBz-KIKO vectors to generate bispecific CAR-T cells (Supplementary Fig. 7d). Five days after electroporation and transduction, FACS analysis revealed that one transduction generated dual knock-in of CD22BBz$^+$CD19BBz$^+$ double-positive CAR-T cells at a bulk efficiency of 21.70%, with CD22BBz$^+$ and CD19BBz$^+$ single-positive cells at bulk efficiency of 22.53% and 7.27%, respectively (Supplementary Fig. 7e,f). All T cells that underwent integration (Q1, Q2, and Q3) had near-complete TCR disruption (Supplementary Fig. 7g). These results demonstrated one-step modular generation of engineered T cells with CD19BBz and CD22BBz double-knock-in and simultaneous *TRAC*;*PDCD1* dual-disruption.

Comparing AAV–Cpf1 KIKO with Cas9-mediated single- and double-knock-in CAR-T cell generation. We then compared the AAV–Cpf1 KIKO platform with Cas9-mediated CAR-T cell generation by targeting the same CAR transgenes into the same loci. We first used Cas9 ribonucleoprotein (RNP) with annealed crRNA and tracrRNA for electroporation to introduce double-stranded breaks, then infected with AAVs carrying CAR HDR templates. This generated knock-in for CD22BBz CAR into the *TRAC* locus (CAR22), with an average of 44.40% CAR22$^+$ T cells on day 5 (Supplementary Fig. 8a,b). This result was confirmed with two independent *PDCD1* guide RNAs (Supplementary Fig. 8b). We also demonstrated CD19BBz CAR knock-in into the *PDCD1* locus (CAR19) similarly (Supplementary Fig. 8c,d). We then performed double-knock-in using Cas9 RNP electroporation followed by AAV infection with both CD22BBz and CD19BBz HDR templates. In parallel, we carried out the AAV–Cpf1 KIKO pipeline, namely, Cpf1 mRNA electroporation followed by infection of AAVs with crTRAC;crPDCD1 as well as CD22BBz and CD19BBz HDR templates. Notably, the AAV–Cpf1 KIKO double-knock-in pipeline efficiently generated CAR19$^+$CAR22$^+$ double-positive cells averaging 35.80% on day 8 (Fig. 4a and Supplementary Fig. 9a), whereas the Cas9 RNP double-knock-in pipeline generated only 3.20% (Fig. 4b and Supplementary Fig. 9b). Using different guide RNAs did not change the efficiency of CAR19$^+$CAR22$^+$ double-knock-in for the Cas9 RNP system (Supplementary Fig. 9c). The frequency of CAR19$^+$CAR22$^+$ double-positive T cells generated by AAV–Cpf1 KIKO in the bulk unsorted population steadily increased from an average of 23.80% on day 5 to 61.73% on day 12 (Fig. 4c), and up to 76.33% on days 14–16 (Supplementary Data 1). CAR19$^+$CAR22$^+$ cells generated by the Cas9 RNP pipeline in the bulk unsorted population averaged 2.56% on day 5 to 4.06% on day 12 (Fig. 4d). Although Cpf1 and Cas9 represent two different nucleases and the two systems do not have strict parity, these data show that, with the current approaches, the AAV–Cpf1 KIKO platform is highly efficient for generating endogenous genomic loci–targeted dual knock-in CAR-T cells.

Immunological characteristics of single- and double-knock-in CAR-T cells. We then compared the phenotypes of various CAR-T cells generated by the AAV–Cpf1 KIKO system. We used a cognate cancer cell line, NALM6 ($CD19^+CD22^+$), and generated an NALM6-GL line that stably expressed GFP and luciferase (Supplementary Fig. 10a–c). We determined the cytolytic activity of CAR-T cells at different titration series of effector/target (E/T) ratios in a coculture setting (kill assay). Vector-transduced T cells had minimal cytolytic activity against NALM6-GL cells; in sharp contrast, all three forms of CAR-T cells generated by Cpf1 KIKO (CAR22, CAR19, and CAR22;CAR19 double-knock-in) had strong potency in killing NALM6-GL cancer cells in a dose-dependent manner (Supplementary Fig. 11a). These three forms of CAR-T cells had similar cytolytic activity (Supplementary Fig. 11a). We then measured the effector cytokine production and found that all three forms of CAR-T cells had highly boosted interferon (IFN)-γ and tumor necrosis factor (TNF)-α production compared with that of vector-transduced T cells (Supplementary Fig. 11b,c). The CAR22;CAR19 double-knock-in CAR-T cells had relatively higher TNF-α and lower IFN-γ productivity compared with that of their single-knock-in counterparts (Supplementary Fig. 11b,c). Thus, both single- and double-knock-in versions of AAV–Cpf1-KIKO-generated CAR-T cells were robustly functional against cognate cancer cells.

Immunological characteristics of CAR-T cells generated by AAV–Cpf1 KIKO and Cas9-mediated knock-in and knockout. We then examined the immunological characteristics of the CAR-T cells generated by the AAV–Cpf1 KIKO platform in parallel with Cas9-mediated knock-in and knockout (Fig. 5a). We found that the CD22BBz CAR-T cells generated by both AAV–Cpf1 KIKO (Cpf1 KIKO CD22BBz) and Cas9-mediated knock-in and knockout (Cas9 RNP CD22BBz) were highly potent compared with vector-transduced T cells (Fig. 5b). Both Cpf1- and Cas9-generated CAR-T cells were potent IFN-γ and TNF-α producers, at comparable levels (Fig. 5c and Supplementary Fig. 12a). Notably, in contrast to Cas9 RNP CD22BBz cells, the Cpf1 KIKO CD22BBz CAR-T cells expressed lower levels of T-cell exhaustion markers including PD-1, TIGIT, and LAG3 (Fig. 5d and Supplementary Fig. 12b). These experiments demonstrated that the AAV–Cpf1 KIKO CAR-targeting method can generate engineered CAR-T cells with potent effector function and reduced levels of exhaustion with simpler transgene delivery, especially when involving the generation of double-knock-in CAR-T cells. Together with the production efficiency data above, these features suggest that AAV–Cpf1 KIKO is a favorable system for rapid and efficient generation of multi-feature CAR-T cells with genomic precision and modular characteristics.

Discussion

Genome engineering on immune cells such as T cells enables efficient introduction of multiple transgenes into different loci, which can be widely used for studying gene functions in human primary T cells and characterizing mutant phenotypes. For example, the immunological characteristics of native or engineered T cells can be rapidly examined for important genes encoding immune checkpoints, master regulators, or previously unknown targets. The multiplexed knock-in and knockout capability can be harnessed to build various reporters or engineer logical circuitries into immune cells to analyze their endogenous expression or signaling pathways. The KIKO system is in principle broadly applicable to various immune-cell types other than T cells, such as hematopoietic stem cells, dendritic cells, and macrophages. Adoptive transfer studies using these engineered cells can facilitate the study of pathological and therapeutic responses in animal models of diseases such as viral infection, immunological disorders, and cancer.

As a 'living drug', genetically engineered CAR-T cells hold tremendous promise for potent and specific antitumor activity[6–8]. Currently, only two CAR-T platforms (Yescarta (axicabtagene ciloleucel) and Kymriah (tisagenlecleucel)) have received approval from the US Food and Drug Administration for treatment of large B-cell lymphomas such as non-Hodgkin lymphoma and B-cell ALL[4]. Most other leukemias and solid tumors do not have approved CAR-T therapy, although multiple preclinical and clinical studies are ongoing with various forms of CAR-T cells[5]. The generation of CAR-T cells involves primary T-cell isolation, transgene introduction, and expansion[27]. Transduction efficiency, transgene expression levels, and CAR stability or retention are all key to this process. However, in lentiviral or retroviral transduction, CAR-T cells tend to lose their transgenes and therefore the ability to recognize and destroy cancer cells[28]. CRISPR–Cas9-mediated *TRAC* knock-in improved CAR-T cell stability and function[11,15]. The KIKO system uses AAV carrying both Cpf1 crRNA array for flexible multiplexed editing and HDR constructs for the introduction of CAR, thus offering important advantages. This system is readily scalable to high-dimensional CAR-T cell engineering such as dual targeting with two CARs and bispecifics[26,29], as well as the introduction of regulatory proteins such as autoregulatory motifs, kill switches, effector boosters, or dampeners[4].

Given the high efficiency, rapid growth rate, and auto-enriching characteristics of the AAV–Cpf1 KIKO CAR-T cell, a regular blood draw can be used to generate a total number of 300 million CAR-T cells (a typical number for clinical infusion) with a number of electroporation-AAV reactions following in vitro expansion for approximately 2 weeks (Supplementary Data 1)[30]. Although this study provides proof of concept for a method that improves the early steps of CAR-T cell engineering, rigorous evaluation of toxicity profiles and in vivo efficacy testing need to be performed in the future before clinical applications. Given further optimization and in vivo testing, this platform, with its simplicity and modularity, has the potential to be broadly used as a research tool in T-cell engineering, as well as a pipeline for improved 'off-the-shelf' adoptive T-cell therapies in the clinic.

Online content

Any methods, additional references, Nature Research reporting summaries, source data, statements of data availability and associated accession codes are available at https://doi.org/10.1038/s41592-019-0329-7.

Received: 14 September 2018; Accepted: 23 January 2019;
Published online: 25 February 2019

References

1. Garfall, A. L. et al. Chimeric antigen receptor T cells against CD19 for multiple myeloma. *N. Engl. J. Med.* **373**, 1040–1047 (2015).
2. Tebas, P. et al. Gene editing of CCR5 in autologous CD4 T cells of persons infected with HIV. *N. Engl. J. Med.* **370**, 901–910 (2014).
3. Jackson, H. J., Rafiq, S. & Brentjens, R. J. Driving CAR T-cells forward. *Nat. Rev. Clin. Oncol.* **13**, 370–383 (2016).
4. Labanieh, L., Majzner, R. G. & Mackall, C. L. Programming CAR-T cells to kill cancer. *Nat. Biomed. Eng.* **2**, 377 (2018).
5. Rosenbaum, L. Tragedy, perseverance, and chance—the story of CAR-T therapy. *N. Engl. J. Med.* **377**, 1313–1315 (2017).
6. Porter, D. L., Levine, B. L., Kalos, M., Bagg, A. & June, C. H. Chimeric antigen receptor–modified T cells in chronic lymphoid leukemia. *N. Engl. J. Med.* **365**, 725–733 (2011).
7. Kalos, M. et al. T cells with chimeric antigen receptors have potent antitumor effects and can establish memory in patients with advanced leukemia. *Sci. Transl. Med.* **3**, 95ra73 (2011). 95ra73.
8. Neelapu, S. S. et al. Axicabtagene ciloleucel CAR T-cell therapy in refractory large B-cell lymphoma. *N. Engl. J. Med.* **377**, 2531–2544 (2017).
9. Themis, M. et al. Oncogenesis following delivery of a nonprimate lentiviral gene therapy vector to fetal and neonatal mice. *Mol. Ther.* **12**, 763–771 (2005).

10. Howe, S. J. et al. Insertional mutagenesis combined with acquired somatic mutations causes leukemogenesis following gene therapy of SCID-X1 patients. *J. Clin. Invest.* **118** 3143–3150 (2008).
11. Eyquem, J. et al. Targeting a CAR to the TRAC locus with CRISPR/Cas9 enhances tumour rejection. *Nature* **543**, 113 (2017).
12. Schumann, K. et al. Generation of knock-in primary human T cells using Cas9 ribonucleoproteins. *Proc. Natl. Acad. Sci. USA* **112**, 10437–10442 (2015).
13. Roth, T. L. et al. Reprogramming human T cell function and specificity with non-viral genome targeting. *Nature* **559**, 405 (2018).
14. Bak, R. O., Dever, D. P. & Porteus, M. H. CRISPR/Cas9 genome editing in human hematopoietic stem cells. *Nat. Protoc.* **13**, 358 (2018).
15. Ren, J. et al. A versatile system for rapid multiplex genome-edited CAR T cell generation. *Oncotarget* **8**, 17002 (2017).
16. Liu, X. et al. CRISPR-Cas9-mediated multiplex gene editing in CAR-T cells. *Cell Res.* **27**, 154 (2017).
17. Zetsche, B. et al. Multiplex gene editing by CRISPR–Cpf1 using a single crRNA array. *Nat. Biotechnol.* **35**, 31 (2017).
18. Kleinstiver, B. P. et al. Genome-wide specificities of CRISPR-Cas Cpf1 nucleases in human cells. *Nat. Biotechnol.* **34**, 869 (2016).
19. Zetsche, B. et al. Cpf1 is a single RNA-guided endonuclease of a class 2 CRISPR-Cas system. *Cell* **163**, 759–771 (2015).
20. Li, B. et al. Engineering CRISPR-Cpf1 crRNAs and mRNAs to maximize genome editing efficiency. *Nat. Biomed. Eng.* **1**, 0066 (2017).
21. Torikai, H. et al. A foundation for universal T-cell based immunotherapy: T cells engineered to express a CD19-specific chimeric-antigen-receptor and eliminate expression of endogenous TCR. *Blood* **119**, 5697–5705 (2012).
22. Kim, H. et al. Surrogate reporters for enrichment of cells with nuclease-induced mutations. *Nat. Methods* **8**, 941 (2011).
23. Rafiq, S. et al. Targeted delivery of a PD-1-blocking scFv by CAR-T cells enhances anti-tumor efficacy in vivo. *Nat. Biotechnol.* **36**, 847–856 (2018).
24. Ren, J. et al. Multiplex genome editing to generate universal CAR T cells resistant to PD1 inhibition. *Clin. Cancer Res.* **23**, 2255–2266 (2017).
25. Haso, W. et al. Anti-CD22-chimeric antigen receptors targeting B-cell precursor acute lymphoblastic leukemia. *Blood* **121**, 1165–1174 (2013).
26. Fry, T. J. et al. CD22-targeted CAR T cells induce remission in B-ALL that is naive or resistant to CD19-targeted CAR immunotherapy. *Nat. Med.* **24**, 20 (2018).
27. Levine, B. L., Miskin, J., Wonnacott, K. & Keir, C. Global manufacturing of CAR T cell therapy. *Mol. Ther. Methods Clin. Dev.* **4**, 92–101 (2017).
28. Ellis, J. Silencing and variegation of gammaretrovirus and lentivirus vectors. *Hum. Gene Ther.* **16**, 1241–1246 (2005).
29. Majzner, R. G. & Mackall, C. L. Tumor antigen escape from CAR T-cell therapy. *Cancer Discov.* **8**, 1219–1226 (2018).
30. Maude, S. L. et al. Chimeric antigen receptor T cells for sustained remissions in leukemia. *N. Engl. J. Med.* **371**, 1507–1517 (2014).

Acknowledgements

We thank C. Fuchs and R. Herbst for their assistance and insightful discussions. We thank L. Ye, J. Li, L. Shen, M. Dong, R. Chow, Z. Bai, X. Zhang, and all other members of the Chen laboratory for technical assistance and discussions. We thank various colleagues in the Department of Genetics, Systems Biology Institute, Cancer Systems Biology Center, MCGD Program, Immunobiology Program, BBS Program, Cancer Center, and Stem Cell Center at Yale for assistance and/or discussion. We thank the Center for Genome Analysis, Center for Molecular Discovery, Pathology Tissue Services, Histology Services, High Performance Computing Center, West Campus Analytical Chemistry Core and West Campus Imaging Core, and Keck Biotechnology Resource Laboratory at Yale for technical support. S.C. is supported by the Yale SBI/Genetics Startup Fund, the Damon Runyon Dale Frey Award (grant/award number DFS-13-15), the Melanoma Research Alliance (412806, 16-003524), St-Baldrick's Foundation (426685), the Breast Cancer Alliance, the Cancer Research Institute (CLIP), AACR (499395, 17-20-01-CHEN), the Mary Kay Foundation (017-81), the V Foundation (V2017-022), the Ludwig Family Foundation, the US Department of Defense (W81XWH-17-1-0235), the Sontag Foundation, the Chenevert Foundation, and the NIH/NCI (1DP2CA238295-01, 1R01CA231112-01, 1U54CA209992-8697, 5P50CA196530-A10805, 4P50CA121974-A08306). G.W. is supported by CRI Irvington and RJ Anderson postdoctoral fellowships. J.J.P. is supported by a Yale MSTP training grant from the NIH (no. T32GM007205).

Author contributions

S.C. conceived the project. X.D. and S.C. designed the project. X.D. performed most experiments with the assistance of Y.D., H.R.K., G.W., and Y.E. J.J.P. developed computational pipelines and performed NGS data analysis. X.D., J.J.P., and S.C. prepared the manuscript. S.C. secured funding and supervised the work.

Competing interests

This research is primarily supported by the Yale SBI/Genetics Startup Fund and the NIH/NCI. The funder has no role in the conceptualization, design, data collection, analysis, decision to publish, or preparation of the manuscript. A provisional patent has been filed by S.C. at Yale University related to this study.

Additional information

Supplementary information is available for this paper at https://doi.org/10.1038/s41592-019-0329-7.

Reprints and permissions information is available at www.nature.com/reprints.

Correspondence and requests for materials should be addressed to S.C.

Publisher's note: Springer Nature remains neutral with regard to jurisdictional claims in published maps and institutional affiliations.

Methods

We developed a protocol for the generation of modular CAR-T cells as detailed in ref. [31].

Institutional approval. This study has received institutional regulatory approval. All recombinant DNA and biosafety work was performed under the guidelines of Yale Environment, Health and Safety Committee with an approved protocol (Chen-rDNA-15-45). All human sample work was performed under the guidelines of Yale University Institutional Review Board with an approved protocol (HIC 2000020784).

T-cell culture. Human primary peripheral blood $CD4^+$ T cells were acquired from healthy donors (STEMCELL Technologies, cat. no. 70026). Cells were obtained using Institutional Review Board–approved consent forms and protocols from the vendor (negative immunomagnetic separation techniques) (STEMCELL Technologies). T cells were cultured in X-VIVO media (Lonza) with 5% human AB (blood type) serum and recombinant human interleukin-2, 30 units (U) ml^{-1}. Before electroporation, T cells were activated with a 1:1 ratio of human anti-CD3/anti-CD28 beads (CD3/CD28 Dynabeads, Thermo Fisher), which were later removed by magnetic separation rack after 2 d.

Generation of LbCpf1 mRNA. Human-codon-optimized LbCpf1 was from ref. [19] and was subcloned into a complementary DNA in vitro transcription vector. Pseudouridine-modified LbCpf1 mRNA with 5′ cap and poly(A) tail was generated from the vector at TriLink.

Construction of AAV vectors. For the generation of an AAV crRNA expression vector (AAV-LbcrRNA, or pXD017), the U6-crRNA expression cassette with double BbsI cutting sites was synthesized and subcloned into an AAV backbone containing inverted terminal repeats. The LbCpf1 crRNA was designed by Benchling to target the first exon of the *TRAC* locus and the second exon of *PDCD1* (Supplementary Table 1). Oligonucleotides (Yale Keck) with sticky ends were annealed, phosphorylated, and ligated into BbsI-digested vector by T4 ligase (NEB). To generate the HDR construct, we amplified the left and right homologous arms of the *TRAC* or *PDCD1* locus by PCR using locus-specific primer sets HDR-F1/R1 and HDR-F2/R2 from primary $CD4^+$ T cells. For transgene cloning, the HDR-R1 and HDR-F2 were connected with a multiple cloning site (Supplementary Table 1). Homologous donor templates were cloned into the AAV-LbcrRNA with or without a crRNA. CD22BBz CAR was generated as previously described[25]. Briefly, the CAR comprises a CD22-binding single chain variable fragment m971 specific for human CD22, followed by CD8 hinge-transmembrane regions linked to 4-1BB (CD137) intracellular domains and CD3ζ intracellular domain. Based on a pXD017-dTomato backbone, m971-BBz was cloned into this vector using a gBlock (IDT). To generate CD19BBz CAR, we found the sequence of CD19-binding single-chain variable fragment (scFv) (FMC63) in NCBI (GenBank, HM852952) and used CD8 hinge-transmembrane regions linked to 4-1BB (CD137) intracellular domains and CD3ζ intracellular domain[32]. To detect CD19BBz CAR in a different way, we added the Flag-tag sequence (GATTACAAAGACGATGACGATAAG) after the CD8-α leader sequence[33]. Based on a pXD017-dTomato backbone, FMC63-BBz was cloned into this vector using a gBlock (IDT). For construction of the HDR template, the EFS-dTomato-PA cassette, EFS-CAR22BBz-PA, or EFS-CAR19BBz-PA cassette was cloned into the multi-clone site.

AAV production and titration. We produced AAV by transfecting HEK293FT cells (Thermo Fisher) in 15-cm tissue culture dishes (Corning). For transfection we used AAV2 transgene vectors, packaging (pDF6) plasmid, and AAV6/9 serotype plasmid together with polyethyleneimine. Transfected cells were collected with PBS 72 h after transfection. For the AAV purification, transfected cells were mixed with pure chloroform (1:10 volume) and incubated at 37 °C with vigorous shaking for 1 h. NaCl was added to a final concentration of 1 M, and then the samples were centrifuged at 20,000*g* at 4 °C for 15 min. The chloroform layer was discarded while the aqueous layer was transferred to another tube. PEG8000 was added to 10% (w/v) and shaken until dissolved. The mixture was incubated at 4 °C for 1 h and then centrifuged at 20,000*g* at 4 °C for 15 min. The supernatant was discarded and the pellet was suspended in Dulbecco's phosphate-buffered saline (DPBS) with $MgCl_2$, treated with universal nuclease (Thermo Fisher), and incubated at 37 °C for 30 min. Chloroform (1:1 volume) was then added, shaken, and centrifuged at 12,000*g* at 4 °C for 15 min. The aqueous layer was isolated and concentrated through a 100-kDa molecular-weight cutoff filter (Millipore). Virus was titered by quantitative PCR using custom Taqman assays (Thermo Fisher) targeted to promoter U6.

T-cell electroporation. Electroporation was performed after T cells were activated for 2 d. After using a magnetic holder to remove CD3/CD28 Dynabeads, we prepared cells at a density of 2×10^5 cells per 10-µl tip reaction or 2×10^6 cells per 100-µL tip reaction in electroporation buffer R (Neon Transfection System Kits). T cells were mixed with 1 µg or 10 µg of modified NLS-LbCpf1 mRNA (TriLink) according to reaction volume and electric-shocked at program 24 (1,600 V, 10 ms, and 3 pulses). After electroporation, the cells were transferred into 1 ml of prewarmed X-VIVO media (without antibiotics) immediately. Indicated volumes of AAV at a defined MOI (specified in figure legends) were added to the T cells 2–4 h after electroporation.

Cas9 RNP electroporation. We produced ribonucleoproteins (RNPs) by complexing a two-component single guide RNA (sgRNA) to Cas9, as previously described[13]. In brief, Cas9 guide RNA was designed to target the same sites as Cpf1 crRNA for *TRAC* and *PDCD1* using Benchling (Supplementary Table 1). Cas9 crRNAs and tracrRNAs were chemically synthesized (Dharmacon or IDT) and resuspended in nuclease-free IDTE buffer at a concentration of 160 µM. The crRNA and tracrRNA were mixed at a 1:1 ratio and annealed as an sgRNA in nuclease-free IDTE buffer at 95 °C for 5 min and 37 °C for 10 min. Each guide was annealed separately and mixed as appropriate. RNPs were formed by the addition of SpCas9 nuclease (Dharmacon, IDT) with 80 µM gRNA (1:2 Cas9-to-sgRNA molar ratio) at benchtop for 15 min. RNPs were electroporated immediately after complexing. After 2–4 h, AAV6 was added into cells at MOI = 1×10^5.

Generation of stable cell lines. Lentiviruses including GFP–luciferase reporter genes were produced as described[34]. NALM6 cells (ATCC) were infected with 2× concentrated lentivirus by spinoculation in retronectin-coated (Takara) plates at 800*g* for 45 min at 32 °C. After infection for 2 d, the GFP^+ cells (NALM6-GL) were sorted on a BD FACSAria II. The second round of sorting was performed after culture for an additional 2 d. To test the luciferase expression in NALM6-GL, cells were incubated with 150 µg ml^{-1} D-luciferin (PerkinElmer) and bioluminescence signal intensity was measured by an IVIS system.

Flow cytometry. Surface protein expression was determined by flow cytometry. After electroporation for 5 d, 1×10^6 cells were incubated with allophycocyanin (APC)–CD4, phycoerythrin (PE)/Cy7–TCR (or PE–TCR), and fluorescein isothiocyanate (FITC)–CD3 antibodies (Biolegend) for 30 min. For the CD22BBz CAR, transduced T cells were incubated with 0.2 µg of CD22-Fc (R&D Systems) in 100 µl of PBS for 30 min, and then stained with PE–IgG-Fc (Biolegend). For the CD19BBz CAR detection, the transduced T cells were stained with APC–anti-DYKDDDDK tag (Biolegend). Stained cells were measured and sorted on a BD FACSAria II. For the T-cell exhaustion assay, T cells from various groups were cocultured with NALM6 cells at a 0.5:1 E/T ratio for 24 h. Then, 1×10^6 cells were incubated with 0.2 µg of CD22-Fc (R&D Systems) in 100 µl of PBS for 30 min and then stained with PE–IgG-Fc, PD-1–FITC, TIGIT–APC, and LAG3–Percp/Cy5.5 (Biolegend) for 30 min. After being washed twice, the stained cells were measured and sorted on a BD FACSAria II, and analyzed with FlowJo software version 9.9.4 or 10.3 (Treestar).

Intracellular staining of IFN-γ and TNF-α. Intracellular staining was performed to detect the expression level of IFN-γ and TNF-α. After infection for 4 d, AAV-transduced CD22BBz CAR-T cells were cocultured with NALM6 cells in fresh medium, which was supplied with brefeldin A and 2 ng ml^{-1} interleukin-2. After being incubated for 5 h, T cells were collected and stained for surface CAR. After membrane protein staining, cells were fixed and permeabilized by fixation/permeabilization solution (BD), followed by the addition of anti-IFN-γ–APC or anti-TNF-α–FITC for intracellular staining. After 30 min, the stained cells were washed with BD Perm/Wash buffer and measured on a BD FACSAria II.

T cell/cancer cell coculture (kill assay). NALM6-GL cells (2×10^4) were seeded in a 96-well plate. The modified or control T cells were cocultured with NALM6-GL at indicated E/T ratios for 24 h. We tested cell proliferation by adding 150 µg ml^{-1} D-luciferin (PerkinElmer) into each well. After 5 min, luciferase assay intensity was measured by a plate reader (PerkinElmer).

Analysis of HDR by In-Out PCR. A semiquantitative In-Out PCR was performed as previously described to measure the rates of dTomato or CAR22 m971-BBz integration at the *TRAC* locus[35]. The assay used three primers in one PCR reaction. One primer recognizes a sequence contained in the dTomato or m971-BBz cassette; a second primer binds to genomic sequence outside of this AAV donor; the third primer binds to a sequence of the left *TRAC* homology arm (Supplementary Table 1). This PCR product, designated *TRAC*-HDR, was normalized by comparison to the product resulting from the control with genomic DNA isolated from normal human $CD4^+$ T cells.

Western blotting analysis. Cells were lysed in ice-cold RIPA buffer (Boston BioProducts) containing protease inhibitors (Roche, Sigma) and incubated on ice for 30 min. Protein supernatant was collected after centrifuging at 13,000*g* and 4 °C for 30 min. Protein concentration was determined via the Bradford protein assay (Bio-Rad). Protein samples were separated under reducing conditions on 4–15% Tris-HCl gels (Bio-Rad) and analyzed by western blotting using primary mouse anti-LbCpf1 (Diagenode; 1:3,000) followed by secondary anti-rabbit HRP antibodies (Sigma-Aldrich; 1:10,000). Blots were imaged with an Amersham Imager 600.

Amplicon sequencing. The resultant PCR products were used for Nextera library preparation according to the manufacturer's protocols (Illumina). Briefly, 1 ng

purified PCR product was fragmented and tagged using the Nextera Amplicon Tagment Mix according the to manufacturer's recommendations, after which limited-cycle PCR was carried out with indexing primers and Illumina adaptors. After this amplification, DNA bands were purified with a gel extraction kit (Qiagen). Libraries were sequenced using 100-base-pair (bp) paired-end reads on an Illumina HiSeq 4000 instrument or equivalent, in general generating between 29 million and 74 million reads per library. For indel quantification, paired reads were mapped to the amplicon sequences using BWA-MEM with the -M option. Then, 100-bp reads from the SAM file that fully mapped within a ±75-bp window of the expected cut site within the amplicon were identified (soft-clipped reads were discarded). Indel reads were then identified by the presence of 'I' or 'D' characters in the CIGAR string. Cutting efficiency was quantified as a percentage of indels over total (indel plus WT) reads within the defined window. Indel variant statistics are provided in Supplementary Data 1, and the raw sequencing files are available via SRA (see 'Data availability' section).

HDR mapping. For HDR quantification, FASTQ reads were mapped to possible amplicons on the basis of primer combinations and HDR status. Mapping was performed for full amplicons and for 'informative' amplicons, which were truncated so that 100-bp reads would have at least 20-bp homology with the CAR sequence (or with the other *TRAC* arm, in the case of WT sequences). Informative reads would be used to distinguish WT, NHEJ, and HDR reads with higher confidence. Paired reads were mapped to amplicon sequences using BWA-MEM with the -M flag to generate SAM files. SAMtools was used to convert files to BAM and to sort, index, and generate summary statistics of read counts with the idxstats option. To quantify WT versus NHEJ reads, we took reads that mapped to the "info_nonHDR" sequence (described below) and called reads with indels (I or D characters within the CIGAR string) as NHEJ. Otherwise, we called reads as WT. Read counts were then pooled for downstream analysis. A description of amplicon sequences follows:

- amplicon_nonHDR: full amplicon from F1 and R1 of genomic, WT DNA
- amplicon_CAR_F1: full amplicon from F1 and R1 of expected, integrated CAR
- amplicon_CAR_F2: full amplicon from F2 (primer site within the CAR as opposed to outside) and R1 of expected, integrated CAR
- info_nonHDR: same as amplicon_nonHDR, except truncated to 80 bp of the *TRAC* arms
- info_CAR_F1: same as amplicon_CAR_F1, except truncated to 80 bp of the *TRAC* arms flanking the *TRAC*–CAR interface
- info_CAR_F2: same as amplicon_CAR_F2, except truncated to 80 bp of the *TRAC* arms flanking the *TRAC*–CAR interface (relevant to the right arm only, as F2 is within the CAR sequence)

HDR, NHEJ, and WT scores were calculated as follows:

- info_nonHDR = info_WT + info_NHEJ
- hdr_score = info_CAR_F2/(info_CAR_F2 + info_nonHDR)
- wt_score = info_WT/(info_CAR_F2 + info_nonHDR)
- nhej_score = info_NHEJ/(info_CAR_F2 + info_nonHDR)

HDR statistics are provided in Supplementary Data 1, and the raw sequencing files are available via SRA (see 'Data availability' section).

Standard statistical analysis (non-NGS). Standard data analyses (non-NGS) were performed using regular statistics, whereas NGS data were analyzed with specific pipelines described above. Data comparison between two groups was done by two-tailed unpaired *t*-test or non-parametric Wilcox test, and *P* values and statistical significance were estimated for all analyses. Data comparison between multiple groups with two factors was done by two-way analysis of variance (ANOVA), and *P* values and statistical significance were estimated for all pair-wise comparisons and adjusted for multiple testing. Prism (GraphPad) and RStudio were used for these analyses. All statistics are provided in Supplementary Data 1.

Reporting Summary. Further information on research design is available in the Nature Research Reporting Summary linked to this article.

Code availability

Analytic codes used to generate figures that support the findings of this study will be made available by the corresponding author upon reasonable request.

Data availability

Genome sequencing data are available via SRA/BioProject under accession number PRJNA509600. Plasmids and libraries are being deposited to Addgene. A list of AAV vectors generated and used in this study is provided in Supplementary Table 2. Original and processed data are included in the figures, figure legends, and supplementary materials of this article. Other relevant data and materials that support the findings of this study will be made available by the corresponding author upon reasonable request.

References

31. Dai, X. et al. Rapid modular CAR-T generation with CRISPR/Cpf1 and AAV systems. *Protocol Exchange* https://doi.org/10.1038/protex.2018.139 (2019).
32. Kochenderfer, J. N. et al. Construction and pre-clinical evaluation of an anti-CD19 chimeric antigen receptor. *J. Immunother.* **32**, 689 (2009).
33. Han, C. et al. Desensitized chimeric antigen receptor T cells selectively recognize target cells with enhanced antigen expression. *Nat. Commun.* **9**, 468 (2018).
34. Chen, S. et al. Genome-wide CRISPR screen in a mouse model of tumor growth and metastasis. *Cell* **160**, 1246–1260 (2015).
35. Wang, J. et al. Highly efficient homology-driven genome editing in human T cells by combining zinc-finger nuclease mRNA and AAV6 donor delivery. *Nucleic Acids Res.* **44**, e30 (2016).

nature research

Corresponding author(s): Sidi Chen

Reporting Summary

Nature Research wishes to improve the reproducibility of the work that we publish. This form provides structure for consistency and transparency in reporting. For further information on Nature Research policies, see Authors & Referees and the Editorial Policy Checklist.

Statistical parameters

When statistical analyses are reported, confirm that the following items are present in the relevant location (e.g. figure legend, table legend, main text, or Methods section).

n/a	Confirmed	
☐	☒	The exact sample size (*n*) for each experimental group/condition, given as a discrete number and unit of measurement
☐	☒	An indication of whether measurements were taken from distinct samples or whether the same sample was measured repeatedly
☐	☒	The statistical test(s) used AND whether they are one- or two-sided *Only common tests should be described solely by name; describe more complex techniques in the Methods section.*
☐	☒	A description of all covariates tested
☐	☒	A description of any assumptions or corrections, such as tests of normality and adjustment for multiple comparisons
☐	☒	A full description of the statistics including central tendency (e.g. means) or other basic estimates (e.g. regression coefficient) AND variation (e.g. standard deviation) or associated estimates of uncertainty (e.g. confidence intervals)
☐	☒	For null hypothesis testing, the test statistic (e.g. *F*, *t*, *r*) with confidence intervals, effect sizes, degrees of freedom and *P* value noted *Give P values as exact values whenever suitable.*
☒	☐	For Bayesian analysis, information on the choice of priors and Markov chain Monte Carlo settings
☒	☐	For hierarchical and complex designs, identification of the appropriate level for tests and full reporting of outcomes
☒	☐	Estimates of effect sizes (e.g. Cohen's *d*, Pearson's *r*), indicating how they were calculated
☐	☒	Clearly defined error bars *State explicitly what error bars represent (e.g. SD, SE, CI)*

Our web collection on statistics for biologists may be useful.

Software and code

Policy information about availability of computer code

Data collection	No specific software was used for data collection.
Data analysis	Flow cytometric data was analyzed using FlowJo v9.9.4 and v.10.3. Amplicon sequencing was analyzed using BWA-MEM with the -M option.

For manuscripts utilizing custom algorithms or software that are central to the research but not yet described in published literature, software must be made available to editors/reviewers upon request. We strongly encourage code deposition in a community repository (e.g. GitHub). See the Nature Research guidelines for submitting code & software for further information.

Data

Policy information about availability of data

All manuscripts must include a data availability statement. This statement should provide the following information, where applicable:

- Accession codes, unique identifiers, or web links for publicly available datasets
- A list of figures that have associated raw data
- A description of any restrictions on data availability

Original and processed data are included in the figures, figure legends and supplemental materials of this manuscript. Analytic codes used to generate figures that

support the findings of this study will be available from the corresponding author upon reasonable requests. Analytic codes used to generate figures, other relevant data and materials that support the findings of this study will be available from the corresponding author upon reasonable requests.

Field-specific reporting

Please select the best fit for your research. If you are not sure, read the appropriate sections before making your selection.

☒ Life sciences ☐ Behavioural & social sciences ☐ Ecological, evolutionary & environmental sciences

For a reference copy of the document with all sections, see nature.com/authors/policies/ReportingSummary-flat.pdf

Life sciences study design

All studies must disclose on these points even when the disclosure is negative.

Sample size	Sample size was determined according to the lab's prior work or similar approaches in the field.
Data exclusions	No data was excluded.
Replication	Number of biological replicates (usually n >= 3) are indicated in the figure legends. For all experiments, the findings were replicated in at least two biological replicates.
Randomization	Randomization was not relevant due to the small sample size of replicates.
Blinding	Blinding was not relevant due to the obvious effect of knockin and knockout.

Reporting for specific materials, systems and methods

Materials & experimental systems

n/a	Involved in the study
☒	☐ Unique biological materials
☐	☒ Antibodies
☐	☒ Eukaryotic cell lines
☒	☐ Palaeontology
☒	☐ Animals and other organisms
☐	☒ Human research participants

Methods

n/a	Involved in the study
☒	☐ ChIP-seq
☐	☒ Flow cytometry
☒	☐ MRI-based neuroimaging

Antibodies

Antibodies used	APC-CD4-Clone A161A1-Biolegend-357408 PE/Cy7-TCR-Clone IP26-Biolegend-306719 PE-TCR Biolegend-Clone IP26-Biolegend-306708 FITC-CD3-Clone HIT3a-Biolegend-300306 PE-IgG-Fc-Clone HP6017-Biolegend-409304 PD-1-FITC-Clone EH12.2H7-Biolegend-329904 TIGIT-APC-Clone A15153G-Biolegend-372705 LAG3-Percp/cy5.5-Clone 11C3C65-Biolegend-369312 APC-anti-DYKDDDDK Tag-Clone L5-Biolegend-637308 PerCP/Cyanine5.5 anti-DYKDDDDK Tag-Clone L5-Biolegend-637326 IFNg-APC-Clone 4S.B3-Biolegend-502512 TNFa-FITC-Clone Mab11-Biolegend-502906 Multiple lots of the same antibodies were used and results were consistent. All the antibodies above were used at 1:100 dilution.
Validation	All Antibodies used in this study were validated by the vendor Biolegend and commonly used by the field. Additional antibody validation information can be found at: https://www.biolegend.com https://www.biolegend.com/reproducibility https://www.biolegend.com/nanostring_validation

Eukaryotic cell lines

Policy information about cell lines

Cell line source(s)	HEK293FT cells were acquired from ThermoFisher. NALM6 cell lines were acquired from ATCC (ATCC CRL-3273)
Authentication	Cell lines were authenticated by the commercial vendor.
Mycoplasma contamination	All cell lines used in this study tested negative for mycoplasma contamination.
Commonly misidentified lines (See ICLAC register)	No commonly misidentified lines were used in the study.

Human research participants

Policy information about studies involving human research participants

Population characteristics	Human primary CD4+ T cells were taken from healthy human donors. Certificates are available from STEMCELL TECHNOLOGIES. Population characteristics were not available from because the primary T cell sources were de-identified.
Recruitment	Human primary CD4+ T cells were taken from healthy human donors by STEMCELL TECHNOLOGIES. There is a potential selection bias due to the small number of donors' T cells used, which might slightly affect the viral transduction efficiency. The potential genetic variations in human population, if happen at the targeted loci, might affect gene targeting.

Flow Cytometry

Plots

Confirm that:

☒ The axis labels state the marker and fluorochrome used (e.g. CD4-FITC).

☒ The axis scales are clearly visible. Include numbers along axes only for bottom left plot of group (a 'group' is an analysis of identical markers).

☒ All plots are contour plots with outliers or pseudocolor plots.

☒ A numerical value for number of cells or percentage (with statistics) is provided.

Methodology

Sample preparation	Surface staining for flow cytometry and cell sorting was performed by pelleting cells and resuspending in 50 µL of FACS Buffer (2% FBS in PBS) with antibodies (1:100 dilution) for 30 minutes at 4C in the dark. Cells were washed once in FACS buffer before resuspension. For the intracellular staining, cells were fixe and permeabilized by fixation/permeabilization solution (BD) for 20 min. and resuspending in 50 µL of permeabilization/wash Bufferwith antibodies (1:100 dilution) for 30 minutes at 4C in the dark. Cells were washed once in FACS buffer before resuspension.
Instrument	Flow cytometric analysis was performed on an BD FACSAria II
Software	FlowJo v.10.3 was used for flow ctyometry data analysis.
Cell population abundance	0.1 million of TCR negative cells were sorted. The sorted cells were re-measured by FACS to confirm the purity.
Gating strategy	A lymphocyte gate was defined first from FSC-A v SSC-A. Singlet gates were then defined on FSC-H v FSC-W. Additional gating was performed as described in figure and extended data legends for individual experiments.

☒ Tick this box to confirm that a figure exemplifying the gating strategy is provided in the Supplementary Information.